IWSCFF 2022

Relative State Estimation for LEO Formations with Large Inter-satellite Distances Using Single-Frequency GNSS Receivers

Ahmed Mahfouz*, Davide Menzio†, Florio Dalla-Vedova‡, and Holger Voos§

Relative baseline estimation is an integral part of satellite formation flying missions. GNSS-based relative positioning has been a dominating technology for formation missions in LEO, where very precise estimates could be obtained for formations with small inter-satellite distances ($1 - 10$ km). Larger baselines between the satellites (> 10 km) pose the problem of considerable differences in the ionospheric delays experienced by the signals received by each receiver. This problem could be mitigated by using precise ionospheric-free combinations that could only be obtained by dual-frequency receivers, which is not a cost-efficient option for modern low-cost miniature missions. In this paper, the problem of relative baseline vector estimation is addressed for formation missions with large inter-satellite distances equipped with single-frequency receivers. The problem is approached using the space-proven relatively simple Extended Kalman Filter with an advantageous setting for the observation vector.
keywords: DGNSS, Relative navigation, State estimation, Extended Kalman Filter

1. Introduction

A reliable state estimation subsystem is essential to close the control loop for any control system. Satellites in Low Earth Orbits (LEO) have long relied on Global Navigation Satellite System (GNSS) signals to estimate their position and velocity vectors in real-time, enabling precise orbit maneuvers. Two distinctive GNSS-based positioning schemes are extricated, absolute positioning, and relative positioning.

Absolute positioning aims at estimating the position vector of the receiver with respect to the center of the Earth, either by solely relying on the measurements from that receiver (standalone positioning) or by combining the measurements from the primary receiver and another nearby base receiver with a precisely known position. The latter leverages Differential GNSS (DGNSS) techniques and is unsuitable for space applications. Relative positioning, on the other hand, is after estimating the baseline vector of one receiver with respect to another, conceivably using the GNSS signals collected by these receivers and also leveraging DGNSS techniques. The accuracy of the absolute positioning schemes can vary from a few centimeters to tens of meters[6,12] depending on many factors such as whether DGNSS is incorporated, atmospheric conditions, receiver quality and design features, and signal blockage.

While absolute positioning is a natural choice for one-satellite missions, relative positioning can be essential for multi-satellite ones. Extended Kalman Filters (EKF) have shown to achieve superb estimates with millimeter-level accuracy of the baseline vector for formations with small inter-satellite distances (1-10 km) in Low Earth Orbits (LEO).[2,7,15] Baseline estimation has also been tackled by Kroes et al.[11] for longer inter-satellite distances and could obtain a remarkable accuracy of 1.7 mm. Although the algorithm which requires dual-frequency receivers has not been implemented onboard a formation flying mission, it has been validated by the GRACE mission data (two satellites, 220 km apart). In the case of long baselines, dual-frequency receivers are very important not only to mitigate the huge difference in ionospheric delay between the two receivers but also to help fix the double-difference integer ambiguities. Nevertheless, the construction of precise relative orbit determination algorithms shall be an enabling technology for low-cost satellite formations in LEO, which comprise single-frequency receivers. In[10] a hybrid Extended/Unscentenced Kalman filter is proposed for baseline determination for widely spaced formations equipped with single-frequency GNSS receivers. The algorithm which performs double-difference integer ambiguity resolution could achieve excellent estimations of the baseline vector (2 cm RMS error) using GPS data that was generated by a GNSS receiver emulator for two spacecraft 500 km apart. Although fairly precise for large baselines, this algorithm suffers from slow convergence time (around 1 hour). The late convergence is hypothesised to be due to two factors, the first is the use of integer ambiguity resolution, and the second is related to using the Klobuchar

*University of Luxembourg, Luxembourg, Ahmed.mahfouz@uni.lu
†University of Luxembourg, Luxembourg, Davide.menzio@uni.lu
‡LuxSpace, Luxembourg, dallavedova@luxspace.lu
§University of Luxembourg, Luxembourg, Holger.voos@uni.lu

ionospheric model in conjunction with an estimated term to account for the unmodeled effect of the ionosphere. Indeed, integer ambiguity resolution is a huge contributor to obtaining centimeter precision. To the contrary, however, estimating a correction term for the ionospheric delay without a relevant dynamic model not only makes the filter take long to converge as the filter tries to estimate this parameter, but also renders the use of the Kolbuchar model meaningless as the filter could estimate the total ionospheric delay instead of estimating only a part of it. Moreover, the use of the Klobuchar model can be directly exploited only for GPS-based navigation as the the Klobuchar coefficients are transmitted in the broadcast message. For navigation set-ups that depend on other GNSS systems, the coefficients need to be generated or chosen from a constant set.
In this paper, relative navigation for satellite formations equipped with single-frequency GNSS receivers and with large inter-satellite distance (100-500 km) is investigated using an Extended Kalman Filter (EKF). In this setting, ionospheric delay is the largest disturbance that needs to be filtered out. A simple ionospheric model is used in conjunction with ionospheric-free combinations to achieve relative state estimates without the need to perform integer ambiguity resolution. The ionospheric model adopted in this paper relies on mapping the Vertical Total Electron Content (VTEC) to the Slant Total Electron Content (STEC) based on a modified version of the Lear mapping function.[13]

The relative position and velocity between two spacecraft are to be estimated directly by the filter rather than estimating the absolute states then subtracting them from each other to obtain the baseline position and velocity, hence, nonlinear relative dynamics between the target and the chaser spacecraft are used, and the measurements to be fed to the filter have to be differential measurements (i.e. single difference, double difference, or triple difference).

This research comes as part of the AuFoSat project which aims at developing a toolbox that features autonomous constellation and formation control solutions comprising state estimation and control algorithms. The toolbox is going to be used by LuxSpace which is currently developing its next generation multi-mission microsatellite "Triton-X" to enable affordable satellite applications in LEO. The consideration of a single-frequency receiver is especially interesting for Triton-X as it uses a 12-channel L1 receiver. Although Triton-X onboard GNSS receiver leverages only GPS signals, the proposed navigation scheme can be used with other GNSS receivers.

2. Problem statement

In formation flying missions, estimating the relative position and velocity of a spacecraft with respect to another is of huge interest. In this paper, the relative state estimation is considered for a formation consisting of two spacecraft, a target and a chaser. The two spacecraft are separated by a large distance and are equipped with single-frequency GNSS receivers. An intersatellite link from the target to the chaser is constructed, which allows the position and velocity of the chaser with respect to the target to be estimated. Although only two spacecraft are considered, the state estimation scheme proposed by this paper is applicable to any two spacecraft in a big formation.
To get a clearer understanding of the challenges that face achieving precise baseline estimates for this formation, a brief summary of the observables of a GNSS system is given in the following discussion.

2.1 *Native GNSS measurements*

The ultimate goal of a GNSS system is to measure the distance between the phase center of the GNSS satellite antenna and the phase center of the receiver's antenna. Two main native measurements are obtained by any GNSS receiver that represent this range: the pseudo-range (code) and the carrier phase. The pseudo-range measurement ρ_{PR} is simply the measured travel time of the signal from the GNSS satellite to the receiver multiplied with the speed of light. The pseudo-range measurement is a coarse measurement of the geometric range that can be modeled as follows if the instrumental delay and the multipath effects are ignored:

$$\rho_{PR} = \rho + c\left(\delta t - \delta t^s\right) + \alpha\left(f\right) S + \nu_{PR}, \qquad [1]$$

where ρ is the geometric range, c is the speed of light, δt and δt^s are the GNSS receiver and satellite clock bias from the GNSS time, $\alpha\left(f\right) S$ is the frequency dependent ionospheric delay where $\alpha\left(f\right)$ is the frequency dependant mapping function between the Slant Total Electron Content (STEC) and the signal delay, S is the STEC, and ν_{PR} is the pseudo-range noise. It is important to emphasise that all the necessary parameters to calculate the satellite's clock bias δt^s are transmitted in the broadcast navigation message.

Besides the pseudo-range, the phase of the carrier on which the information are modulated can be used to measure the geometric range between the GNSS satellite and receiver. The carrier phase measurement is much smoother than the pseudo-range,

however, it includes an ambiguous term that results from the unknown integer number of wavelengths and also from the wind-up effect. If the multipath and the instrumental delay are ignore, the carrier-phase measurement can be modelled as:

$$\rho_{CP} = \rho + c\left(\delta t - \delta t^s\right) + \lambda_f N - \alpha\left(f\right) S + \nu_{CP}, \quad [2]$$

where λ_f is the wavelength corresponding to frequency f, N is the floating point ambiguity in cycles, and ν_{CP} is the carrier phase noise. Typically, the carrier phase is two orders of magnitude more precise than the pseudo-range (i.e. $|\nu_{CP}| \approx 0.01\,|\nu_{PR}|$).

2.2 *Differential measurements*

In the context of relative estimation of the states of the chaser with respect to the target, the well known single and double differences can be used. Concretely, the single difference pseudo-range (SDCP) can be obtained by subtracting the carrier-phase measurement of the target from the carrier-phase measurement of the chaser at the same instant and for signals received from a commonly tracked satellite.

$$\rho_{SDCP} \coloneqq \rho_{CP}|_t - \rho_{CP}|_c = \Delta\rho + c\Delta\delta t + \lambda_f \Delta N - \alpha\left(f\right)\Delta S + \nu_{SDCP}, \quad [3]$$

where $\left(\cdot\right)_t$ is a target related quantity, $\left(\cdot\right)_c$ is a chaser related quantity, $\Delta\left(\cdot\right) \coloneqq \left(\cdot\right)_c - \left(\cdot\right)_t$, and $\nu_{SDCP} \sim \mathcal{N}(0, \sigma^2_{SDCP})$ with $\mathcal{N}(\mu, \sigma^2)$ being the normal distribution with a mean μ and a variance σ^2 and $\sigma_{SDCP} \approx \sqrt{2}\sigma_{CP}$.

Double difference quantities can be obtained by subtracting single difference quantities that were collected from two different satellites. Namely, the double difference carrier phase (DDCP) is constructed by subtracting the single difference carrier phase collected from satellite p and q as follows:

$$\rho_{DDCP} \coloneqq \rho^p_{SDCP} - \rho^q_{SDCP} = \Delta^{p,q}\rho + \lambda_f \Delta^{p,q} N - \alpha\left(f\right)\Delta^{p,q} S + \nu_{DDCP}, \quad [4]$$

where $\Delta^{p,q}\left(\cdot\right) \coloneqq \Delta^p\left(\cdot\right) - \Delta^q\left(\cdot\right)$, and $\Delta^p\left(\cdot\right)$ and $\Delta^q\left(\cdot\right)$ are single difference quantities related to the GNSS satellites p and q respectively. It can be deduced that $\nu_{DDCP} \sim \mathcal{N}(0, \sigma^2_{DDCP})$ with $\sigma_{DDCP} \approx 2\sigma_{CP}$.

It can be seen that using differential measurements not only allows the direct estimation of the baseline vector between two receivers, but also features some interesting properties such as cancelled common noises. The most important property of the DDCP is that it is not affected by the wind-up which renders the double difference ambiguity $\Delta^{p,q}N$ integer. This property is usually leveraged in resolving and fixing ambiguities mostly by using the LAMBDA[18] or the MLAMBDA[4] algorithms. Resolving double difference integer ambiguities is a key factor in obtaining precise relative position and velocity estimates.[10,11,17] It is to be stressed that there are various types of differential measurements with different advantages yet, this discussion is out of the scope of this paper. Interested reader is referred to Chapter 6 in.[14]
It is important to note that the single and double difference concepts are not limited to the native measurements, as they are also applicable to the measurement combinations discussed in the next section.

2.3 *Measurements combinations*

When the two receivers are close to each other, the differential ionospheric delay $\alpha\left(f\right)\Delta S$, together with the other noises, become negligible, that is why differential measurements perform adequately even without integer ambiguity resolution.[2,8] However, when the two spaceraft are separated by a large baseline, as is the case of the proposed Triton-X formation, the ionospheric effect becomes the main source of noise, and rigorous ionospheric models need to be used. One way to mitigate this problem is to use ionospheric-free combinations. There are many ionospheric-free combinations that require dual-frequency receivers in order to be realized, nevertheless, for single-frequency receivers, the well-known Group and Phase Ionospheric Correction (GRAPHIC) combination[19] can be used. The GRAPHIC combination is simply the arithmetic mean of the pseudo-range and the carrier phase measurements. It is modeled as:

$$\rho_{GR} \coloneqq \frac{\rho_{PR} + \rho_{CP}}{2} = \rho + c\left(\delta t - \delta t^s\right) + \frac{\lambda_f N}{2} + \nu_{GR}, \quad [5]$$

where $\nu_{GR} \sim \mathcal{N}(0, \sigma^2_{GR})$ with $\sigma_{GR} \approx 0.5\sigma_{PR}$. The advantages of the GRAPHIC combination are not limited to being an ionospheric free combination, as it also experiences lower levels of noise in comparison to the native pseudo-range measurement ($|\nu_{GR}| \approx 0.5\,|\nu_{PR}|$), however, the noise level in the GRAPHIC is still not as low as that of the carrier phase measurement.
Similar to the SDCP, the Single Difference GRAPHIC (SDGR) can be obtained by subtracting the GRAPHIC value for the target spacecraft from that of the chaser

spacecraft,

$$\rho_{SDGR} \coloneqq \rho_{GR}|_t - \rho_{GR}|_c = \Delta\rho + c\Delta\delta t + \frac{\lambda_f \Delta N}{2} + \nu_{SDGR}, \quad [6]$$

where $\nu_{SDGR} \sim \mathcal{N}(0, \sigma^2_{SDGR})$ with $\sigma_{SDGR} \approx \sigma_{PR}/\sqrt{2}$.

One other interesting linear combination of the GNSS native measurements is the Geometric Free ionospheric combination (GF) which results from subtracting the carrier phase from the pseudo-range. It can be modelled according to [1] and [2] as:

$$\rho_{GF} \coloneqq \rho_{PR} - \rho_{CP} = 2\alpha(f)\, S - \lambda_f N + \nu_{GF}. \quad [7]$$

Again, the Single Difference Geometric Free combination can be obtained the same way as for pseudo-range, carrier phase, and GRAPHIC,

$$\rho_{SDGF} \coloneqq \rho_{GF}|_t - \rho_{GF}|_c = 2\alpha(f)\,\Delta S - \lambda_f \Delta N + \nu_{SDGF}, \quad [8]$$

where $\nu_{SDGF} \sim \mathcal{N}(0, \sigma^2_{SDGF})$ with $\sigma_{SDGF} \approx \sqrt{2}\sigma_{PR}$.

The linear combinations of measurements discussed in this section can be used individually or concurrently to estimate the relative position of the receivers as well as the auxiliary quantities such as the differential clock bias Δt, the differential ionospheric delay $\alpha(f)\,\Delta S$, or the differential float ambiguity ΔN.

2.4 *Extended Kalman Filter algorithm*

While the choice of the measurement combinations to be fed to the filter might be an exhausting task, this is not the case for the choice of the estimation algorithm, as the Extended Kalman Filter (EKF) is a space proven algorithm that has been used for decades. The extended Kalman Filter (EKF) is an extension of the well-known Kalman Filter (KL) that combines information from the process and the observation models which can be nonlinear models of the state,

$$\boldsymbol{X}_k = \boldsymbol{f}(\boldsymbol{X}_{k-1}, \boldsymbol{u}_k) + \boldsymbol{w}_k, \quad [9]$$

$$\boldsymbol{z}_k = \boldsymbol{h}(\boldsymbol{X}_k) + \boldsymbol{\nu}_k. \quad [10]$$

Equations [9] and [10] are the state transition and the measurement models respectively. The vector $\boldsymbol{X}_k$ represents the state vector at time instant k which is to be estimated by the EKF, $\boldsymbol{u}_k$ is the known/estimated input vector, and $\boldsymbol{w}_k$ and $\boldsymbol{\nu}_k$ are the process and the measurement noises respectively which are normally distributed multivariate random variables, with $\boldsymbol{w}_k \sim \mathcal{N}(\boldsymbol{0}, \mathbb{Q}_k)$ and $\boldsymbol{\nu}_k \sim \mathcal{N}(\boldsymbol{0}, \mathbb{R}_k)$.

The EKF is usually divided into two successive phases, the prediction and the update. In the sequel, the hat symbol $\hat{(\cdot)}$ signifies a quantity that is produced by the filter (i.e. an estimation), while the double subscript $(\cdot)_{m|n}$ represents the estimation of $(\cdot)$ at the time instant m given the measurements up to and including the time instant n, where $n < m$.

The prediction phase is depicted in the following set of equations,

$$\begin{aligned} \hat{\boldsymbol{X}}_{k|k-1} &= \boldsymbol{f}\left(\hat{\boldsymbol{X}}_{k-1|k-1}, \boldsymbol{u}_k\right) \\ \hat{\mathbb{P}}_{k|k-1} &= \mathbb{F}_k \hat{\mathbb{P}}_{k-1|k-1} \mathbb{F}_k^\intercal + \mathbb{Q}_k, \end{aligned} \quad [11]$$

where $(\cdot)^\intercal$ is the matrix transpose, and

$$\mathbb{F}_k \coloneqq \left.\frac{\partial \boldsymbol{f}}{\partial \boldsymbol{X}}\right|_{\hat{\boldsymbol{X}}_{k-1|k-1},\, \boldsymbol{u}_k}.$$

The update phase can as well be summarised by the following equations:

$$\begin{aligned} \mathbb{K}_k &= \hat{\mathbb{P}}_{k|k-1} \mathbb{H}_k^\intercal \left(\mathbb{H}_k \hat{\mathbb{P}}_{k|k-1} \mathbb{H}_k^\intercal + \mathbb{R}_k\right)^{-1} \\ \hat{\boldsymbol{X}}_{k|k} &= \hat{\boldsymbol{X}}_{k|k-1} + \mathbb{K}_k \left(\boldsymbol{z}_k - \boldsymbol{h}\left(\hat{\boldsymbol{X}}_{k|k-1}\right)\right) \\ \hat{\mathbb{P}}_{k|k} &= \left(\mathbb{I} - \mathbb{K}_k \mathbb{H}_k\right) \hat{\mathbb{P}}_{k|k-1}, \end{aligned} \quad [12]$$

where

$$\mathbb{H}_k \coloneqq \left.\frac{\partial \boldsymbol{h}}{\partial \boldsymbol{X}}\right|_{\hat{\boldsymbol{X}}_{k|k-1}}.$$

3. Extended Kalman Filter set-up

This section is dedicated to introducing the state variables to be estimated by the EKF as well as the measurement combinations to be fed to the filter in the update phase.

Clearly, the main variables that need to be estimated are the baseline vector and the relative velocity between two spacecraft, however, some auxiliary variables (e.g. receiver's clock bias, carrier phase float ambiguities,...) need to be estimated in order to increase the precision of the filter. In fact, if an EKF filter is run without accounting for these auxiliary variables, especially the receiver's clock bias, it is susceptible to generate unusable estimates.

In the domain of GNSS-based relative state estimation, a unique set of state variables does not exist, and the choice of the state vector is customary. In fact, the choice of the state variables to be estimated is heavily dependant on the choice of the measurements

combinations to be fed to the filter, which itself is customary.
A brief study was carried out in order to help asses the effectiveness of using different sets of state variables in conjunction with different sets of measurement combinations, and highlights of this preliminary study are presented in Table 1.

In Table 1, $\Delta\boldsymbol{r}$ and $\Delta\boldsymbol{v}$ are the relative position and velocity vectors respectively, while n refers to the number of independent channels in the used GNSS receiver. By no ionospheric model we mean that the term $\alpha(f)\Delta S$ in [3] and [8] is estimated directly by the filter for each of the commonly visible satellites, while the Lear ionospheric model is discussed later in **Section 4**. The proposition of not including an ionospheric model is a common practice in the literature (see for example[11]), however, it could lead to a late convergence of the filter, which is obvious in Table 1.

The preliminary results helped conclude that the inclusion of an ionospheric model could not only dramatically improve the convergence rate of the filter, but also improve the overall precision of the velocity estimates. It also helped conclude that the advantages of the SDGR, the SDCP, and the SDGF combinations, defined in equations [6], [3], and [8] respectively, are worth exploiting.
The measurement vector $\boldsymbol{z}$ in equation [10] could then be constructed as:

$$\boldsymbol{z} \coloneqq \begin{bmatrix} \boldsymbol{\rho}_{SDGR} \\ \boldsymbol{\rho}_{SDCP} \\ \boldsymbol{\rho}_{SDGF} \end{bmatrix}. \qquad [13]$$

It is to be noted that $\boldsymbol{\rho}_{SDGR}$, $\boldsymbol{\rho}_{SDCP}$, and $\boldsymbol{\rho}_{SDGF}$ are no longer scalar values that correspond to one GNSS satellite, but rather vectors that comprise the measured combinations from all the commonly tracked satellites. In this setting, the length of the measurement vector is $3n$, where n is the number of channels of the GNSS receiver (12 channels for the Triton-X onboard receiver).
The choice of this measurement vector is not arbitrary, at least it was not arbitrary to try out these combinations in our preliminary study, and the reasons for this choice are listed below:

1. The relative position and velocity of one spacecraft with respect to another are estimated directly by the filter, instead of estimating the absolute states of the two spacecraft then subtract the state vector of one spacecraft from that of the other. In this setting, differential measurements have to be used, hence the single difference combinations are chosen.

2. As the ionospheric delay is the most significant noise to be accounted for, the use of ionospheric-free combinations comes as no surprise. That is why the SDGR is used, as GRAPHIC is the only known single-frequency ionospheric-free combination.

3. Although the SDGR is an ionospheric-free combination, it is still a noisy measurement, that is why more precise combinations, like the SDCP, need to be included to augment the overall accuracy of the filter. It has to be noted that the inclusion of the SDCP comes with its own challenges, like having to estimate the ionospheric effect as well as the float ambiguities.

4. It was believed from the beginning that the inclusion of the ionospheric geometric-free combination, the SDGF, shall assist in estimating the ionospheric delay as well as the ambiguities however being coarse. This hypothesis was tested true by the preliminary study results in Table 1.

Having chosen the measurement vector, the state vector $\boldsymbol{X}$ can now be constructed based on the chosen measurements. The choice of the state variables for this research is,

$$\boldsymbol{X} \coloneqq \begin{bmatrix} \Delta\boldsymbol{x}^\intercal & c\Delta\delta t & c\dot{\Delta}\delta t & \boldsymbol{V}_c^\intercal & \boldsymbol{V}_t^\intercal & \Delta\boldsymbol{N}^\intercal \end{bmatrix}^\intercal, \qquad [14]$$

where $\boldsymbol{x} \coloneqq \begin{bmatrix} \boldsymbol{r}^\intercal & \boldsymbol{v}^\intercal \end{bmatrix}^\intercal$ is the vector that contains the position and velocity coordinates of a receiver in the Earth-Centred, Earth-Fixed (ECEF) frame, $\Delta\delta t$ is the differential receiver's clock bias with $\dot{\Delta}\delta t$ being its rate of change, $\boldsymbol{V}_c$ and $\boldsymbol{V}_t$ are the Vertical Total Electron Content (VTEC) vectors of the chaser and the target spacecraft respectively containing all the VTECs for all the commonly visible satellites, and $\boldsymbol{N}$ is the carrier phase float ambiguity vector for all the commonly tracked satellites by the chaser and target.
For a given tracked signal that travels from the GNSS satellite to the receiver, the VTEC, V, can be empirically mapped to the STEC, S, through the following simple mapping:

$$S = m(\varepsilon)\, V, \qquad [15]$$

where $m(\varepsilon)$ is a mapping function of the elevation angle ε of the GNSS satellite with respect to the receiver. The details of the mapping function are to be discussed in **Section 4**.
The length of the state vector in this setting is $8+3n$, where n is the number of channels of the GNSS receiver (12 channels for Triton-X onboard receiver). The $\Delta\boldsymbol{x}$ vector accounts for 6 state variables, $c\Delta\delta t$

#	Measurements	Ionospheric model	# states	RMS error in $\|\Delta\boldsymbol{r}\|$ (cm)	RMS error in $\|\Delta\boldsymbol{v}\|$ (cm/s)	Convergence time (min)
1	SDGR	N/A	$8+n$	86	20	0.37
2	SDCP	None	$8+2n$	312	19	83.9
3	DDCP	None	$8+2n$	310	19	83.9
4.1	SDGR + SDCP	None	$8+2n$	48	18	32.7
4.2	SDGR + SDCP	Lear	$8+3n$	61	9	0.05
5.1	SDCP + SDGF	None	$8+2n$	45	18	27
5.2	SDCP + SDGF	Lear	$8+3n$	47	9	0.15

Table 1: Summary of the preliminary results for 22 hours of the SWARM mission data

and $c\Delta\dot{\delta}t$ add two more variables, while each of $\boldsymbol{V}_c$, $\boldsymbol{V}_t$, and $\Delta\boldsymbol{N}$ account for n variables.

Choosing to estimate the VTEC for the chaser and the target separately instead of estimating $\Delta\boldsymbol{V}$ stems from the fact that $\Delta\boldsymbol{V}$ never appears explicitly in the measurement model [6], [3], and [8], unlike the quantity ΔN which appears explicitly in the measurement model. Only if the elevation angle of the common GNSS satellite can be assumed to be the same for the two receivers is it possible to estimate the single difference VTEC, $\Delta\boldsymbol{V}$, directly. This assumption can only be valid for small baselines between the two receivers. In this case, the quantity $\Delta\boldsymbol{V}$ explicitly appears in the measurement model.

4. Dynamical models

In this section, the dynamical models (e.g. $\boldsymbol{f}$) together with the Jacobian matrices (e.g. $\mathbb{F}_k$ and $\mathbb{H}_k$) necessary for the operation of the EKF are presented. The dynamics of the state vector are separated into the orbital dynamics, concerning the $\Delta\boldsymbol{x}$ vector, and the dynamics of the auxiliary variables which concern the rest of the state variables in [14].

4.1 *Relative orbital dynamics*

The absolute dynamics of a satellite moving under the influence of the gravity of the Earth can be described by,

$$\ddot{\boldsymbol{r}} = -\frac{\mu}{r^3}\boldsymbol{r} + \boldsymbol{\omega}_e \times \boldsymbol{v} + \boldsymbol{\omega}_e \times \boldsymbol{\omega}_e \times \boldsymbol{r} + \boldsymbol{u} + \boldsymbol{w}_{\boldsymbol{v}}, \quad [16]$$

where $\boldsymbol{r}$, $\boldsymbol{v}$, $\boldsymbol{u}$, and $\boldsymbol{w}_{\boldsymbol{v}}$ are the position, velocity, control, and disturbance vectors respectively in the ECEF frame, $\boldsymbol{\omega}_e \approx \begin{bmatrix}0 & 0 & \omega_e\end{bmatrix}^\intercal$ is the rotational velocity vector of the Earth, and μ is the standard gravitational parameter of the Earth.

The relative orbital dynamics between the chaser and the target spacecraft in the ECEF frame can be simply dervied from [16],

$$\begin{aligned}
\Delta\dot{\boldsymbol{x}} &:= \begin{bmatrix}\Delta\dot{\boldsymbol{r}}^\intercal & \Delta\dot{\boldsymbol{v}}^\intercal\end{bmatrix}^\intercal, \\
\Delta\dot{\boldsymbol{r}} &= \Delta\boldsymbol{v}, \\
\Delta\dot{\boldsymbol{v}} &= \frac{\mu}{r_t^3}\left(\boldsymbol{r}_t - \frac{r_t^3\left(\boldsymbol{r}_t + \Delta\boldsymbol{r}\right)}{\left(r_t^2 + 2\boldsymbol{r}_t\cdot\Delta\boldsymbol{r} + \Delta r^2\right)^{3/2}}\right) \\
&\quad + \boldsymbol{\omega}_e \times \boldsymbol{\omega}_e \times \Delta\boldsymbol{r} + \boldsymbol{\omega}_e \times \Delta\boldsymbol{v} \\
&\quad + \Delta\boldsymbol{u} + \boldsymbol{w}_{\Delta\boldsymbol{v}},
\end{aligned} \quad [17]$$

where $\boldsymbol{r}_t$ is the position vector of the target satellite in the ECEF frame with a magnitude of r_t, $\Delta\boldsymbol{r}$ and $\Delta\boldsymbol{v}$ are the relative position and velocity vectors respectively from the target to the chaser spacecraft with magnitudes of Δr and Δv. Moreover, $\Delta\boldsymbol{u} = \boldsymbol{u}_c - \boldsymbol{u}_t$ is the differential control vector, and $\boldsymbol{w}_{\Delta\boldsymbol{v}}$ collates all the relative acceleration noises, $\boldsymbol{w}_{\Delta\boldsymbol{v}} \sim \mathcal{N}\left(\boldsymbol{0}, \mathbb{Q}_{\Delta\boldsymbol{v}}\right)$.

In the prediction phase of the EKF [11], equation [17] is numerically integrated after omitting the disturbance, to obtain a prediction of the relative position and velocity states where the initial condition for the this integration is drawn from the estimated state vector.
It is of a huge interest to obtain predictions of the absolute position and velocity vectors of each spacecraft as these vectors are essential for the operation of the EKF. Instead of numerically integrating the absolute dynamical equations [16], the absolute states are directly acquired from the receiver's noisy onboard solution at each measurement step. This solution can be used as an initial condition for the integration of

the absolute dynamics if necessary. The onboard solution of Triton-X onboard receiver is characterized by a noise level of 10 m for the position and 25 cm/s for the velocity (1σ), which are acceptable noise levels as the onboard solution is only used in calculating the Jacobian matrices required by the EKF, and not in propagating the state variables.

4.2 *State transition matrix*

With the definition of the state variables [14] in mind, the State Transition Matrix (STM) ($\mathbb{F}_k$ in [11]) can be divided into several sub-matrices as,

$$\begin{aligned}\mathbb{F} &\coloneqq \frac{\partial \boldsymbol{X}_k}{\partial \boldsymbol{X}_{k-1}} \\ &= \operatorname{diag}\left(\mathbb{F}_{\Delta\boldsymbol{x}}, \quad \mathbb{F}_{c\Delta\delta t}, \quad \mathbb{F}_{\boldsymbol{V}_c}, \quad \mathbb{F}_{\boldsymbol{V}_t}, \quad \mathbb{F}_{\Delta\boldsymbol{N}}\right)\end{aligned} \tag{18}$$

where $\mathbb{F}_{\Delta\boldsymbol{x}}$, $\mathbb{F}_{c\Delta\delta t}$, $\mathbb{F}_{\boldsymbol{V}_c}$, $\mathbb{F}_{\boldsymbol{V}_t}$, and $\mathbb{F}_{\Delta\boldsymbol{N}}$ are the state transition matrices for $\Delta\boldsymbol{x}$, $c\Delta\delta t$, $\boldsymbol{V}_c$, $\boldsymbol{V}_t$, and $\Delta\boldsymbol{N}$ respectively. Moreover, $\operatorname{diag}(\ldots)$ is a function which places its input arguments on the diagonal of the output matrix with zero off diagonal entries.

Various linearization techniques can be adopted in order to obtain the STM $\mathbb{F}_{\Delta\boldsymbol{x}}$,[3] nonetheless, this STM is not used to propagate the states, but rather to propagate the estimated states variance-covariance matrix (as seen in [11]), hence the constraint of having a very precise STM becomes much looser. The simple STM obtained from the closed form solution to the Clohessy–Wiltshire (CW) equations[5] can be used, however, one needs to keep an eye on the fact that CW equations provide the solution in Hill's frame of the target spacecraft, and the obtained STM has to be rotated to the ECEF. In this paper, an even simpler approach is adopted by linearizing the equations of motion [17] taking the target's orbit as a reference for the linearization. In this case, the STM of the relative states $\mathbb{F}_{\Delta\boldsymbol{x}}$ is only dependent on the target's states. Approximating the Jacobian of the relative states by the Jacobian of the target's states yields,

$$\begin{aligned}\mathbb{J} &\coloneqq \frac{\partial \Delta\dot{\boldsymbol{x}}}{\partial \Delta\boldsymbol{x}} \approx \left.\frac{\partial \dot{\boldsymbol{x}}}{\partial \boldsymbol{x}}\right|_{\boldsymbol{x}=\boldsymbol{x}_t}, \\ \mathbb{F}_{\Delta\boldsymbol{x}} &\coloneqq \frac{\partial \Delta\boldsymbol{x}_k}{\partial \Delta\boldsymbol{x}_{k-1}} \approx \mathbb{I}_6 + (t_k - t_{k-1})\,\mathbb{J}|_{\boldsymbol{x}_t|_{k-1}},\end{aligned} \tag{19}$$

where $\mathbb{I}_6$ is the identity matrix of size 6, t_k and t_{k-1} are the two consecutive time instants to which the STMs correspond, $\mathbb{J}$ is the state-dependant Jacobian matrix that can be calculated by partial differentiation of [16], and $\mathbb{J}|_{\boldsymbol{x}_t|_{k-1}}$ is the Jacobian matrix evaluated at the target's state at time t_{k-1}.

The rest of the variables are modeled as random walk processes,

$$\begin{aligned} c\ddot{\Delta\delta t} &= w_{c\dot{\Delta\delta t}}, \\ \dot{\boldsymbol{V}}_c &= \boldsymbol{w}_{\boldsymbol{V}_c}, \\ \dot{\boldsymbol{V}}_t &= \boldsymbol{w}_{\boldsymbol{V}_t}, \\ \dot{\Delta\boldsymbol{N}} &= \boldsymbol{0}, \end{aligned} \tag{20}$$

where $w_{c\dot{\Delta\delta t}} \sim \mathcal{N}\left(0, \sigma^2_{c\dot{\Delta\delta t}}\right)$, $\boldsymbol{w}_{\boldsymbol{V}_c} \sim \mathcal{N}(\boldsymbol{0}, \mathbb{Q}_{\boldsymbol{V}})$, and $\boldsymbol{w}_{\boldsymbol{V}_t} \sim \mathcal{N}(\boldsymbol{0}, \mathbb{Q}_{\boldsymbol{V}})$, with $\mathbb{Q}_{\boldsymbol{V}}$ being the variance-covariance matrix of a VTEC vector.

The state transition matrices of the auxiliary variables can be directly derived from the linear system of equations [20] after omitting the noise as follows:

$$\begin{aligned} \mathbb{F}_{c\Delta\delta t} &= \begin{bmatrix} 1 & t_k - t_{k-1} \\ 0 & 1 \end{bmatrix}, \\ \mathbb{F}_{\boldsymbol{V}_c} &= \mathbb{F}_{\boldsymbol{V}_t} = \mathbb{F}_{\Delta\boldsymbol{N}} = \mathbb{I}_n, \end{aligned} \tag{21}$$

where $\mathbb{I}_n$ is the identity matrix of size n, with n being the number of channels of the adopted GNSS receiver. Equation [21] not only can be used to construct the full STM [18], but also to propagate the auxiliary states in the prediction phase of the EKF [11].

4.3 *Measurement model*

Although the measurement vector in [13] is modeled by equations [6], [3], and [8], the Jacobian matrix $\mathbb{H}$ of these nonlinear functions needs to be determined as a requirement for the update phase of the EKF [12]. Concretely, the nonlinear measurement model is presented once again as follows,

$$\boldsymbol{h}(\boldsymbol{X}) = \begin{bmatrix} \Delta\boldsymbol{\rho} + c\Delta\delta t + \frac{\lambda_f}{2}\Delta\boldsymbol{N} \\ \Delta\boldsymbol{\rho} + c\Delta\delta t + \lambda_f\Delta\boldsymbol{N} - \alpha(f)\,\Delta\boldsymbol{S} \\ 2\alpha(f)\,\Delta\boldsymbol{S} - \lambda_f\Delta\boldsymbol{N} \end{bmatrix}, \tag{22}$$

where the differential STEC vector $\Delta\boldsymbol{S}$ is obtained from the VTEC vectors according to the mapping [15], $\Delta\boldsymbol{S} = \boldsymbol{m}(\boldsymbol{\varepsilon}_c)\,\boldsymbol{V}_c - \boldsymbol{m}(\boldsymbol{\varepsilon}_t)\,\boldsymbol{V}_t$.

The state dependant Jacobian matrix $\mathbb{H}$ can then be obtained,

$$\mathbb{H}(\boldsymbol{X}) = \begin{bmatrix} \mathbb{E} & \mathbb{0} & \mathbf{1} & \mathbf{0} & \mathbb{0} & \mathbb{0} & \frac{\lambda_f}{2}\mathbb{D} \\ \mathbb{E} & \mathbb{0} & \mathbf{1} & \mathbf{0} & -\boldsymbol{b}_c^\intercal\mathbb{D} & \boldsymbol{b}_t^\intercal\mathbb{D} & \lambda_f\mathbb{D} \\ \mathbb{0} & \mathbb{0} & \mathbf{0} & \mathbf{0} & 2\boldsymbol{b}_c^\intercal\mathbb{D} & -2\boldsymbol{b}_t^\intercal\mathbb{D} & -\lambda_f\mathbb{D} \end{bmatrix}, \tag{23}$$

where $\boldsymbol{b}_c \coloneqq \alpha(f)\,\boldsymbol{m}(\boldsymbol{\varepsilon}_c)$, $\boldsymbol{b}_t \coloneqq \alpha(f)\,\boldsymbol{m}(\boldsymbol{\varepsilon}_t)$, and $\mathbb{D}$ is a Boolean rearrangement matrix that is in general not square. Moreover, Matrix $\mathbb{E}$ in [23] is itself a Jacobian matrix that is obtained by linearizing the $\Delta\boldsymbol{\rho}$ part

of the measurement model around the states of the target, and similar to [19], this matrix depends only on the target's states,

$$\mathbb{E} \coloneqq \frac{\partial \Delta \boldsymbol{\rho}}{\partial \Delta \boldsymbol{r}} \approx \frac{\partial \boldsymbol{\rho}_t}{\partial \boldsymbol{r}_t} = \begin{bmatrix} \boldsymbol{e}_t^1 & \boldsymbol{e}_t^2 & \dots & \boldsymbol{e}_t^m & \mathbf{0} & \dots & \mathbf{0} \end{bmatrix}^\intercal, \quad [24]$$

where the zero vectors at the end account for the target's receiver channels that did not track any satellite or that tracked a satellite that is not visible by the chaser, $\boldsymbol{e}_t^p$ is the unit baseline vector between the target and the p^{th} commonly tracked satellite in the ECEF frame, with m being the number of commonly tracked satellites. Namely,

$$\boldsymbol{e}_t^p = \frac{\boldsymbol{r}_t - \boldsymbol{r}^p}{\|\boldsymbol{r}_t - \boldsymbol{r}^p\|}. \quad [25]$$

4.4 *Ionospheric model*

Besides estimating the VTEC vectors by the filter, one has to define the two mapping functions $\alpha(f)$ and $m(\varepsilon)$ given in [1] and [15] respectively in order to estimate the ionospheric delay that affects a signal.

The frequency dependent mapping function that maps the STEC to the ionospheric delay $\alpha(f)$ is modeled by the following formula,[1]

$$\alpha(f) = \frac{40.3 \cdot 10^{16}}{f^2} \text{ m/TECU}, \quad [26]$$

where f is the carrier frequency in Hz, which for GPS L1 is equal to 1575.42 MHz, and TECU is the Total Electrol Content Unit (TECU $= 10^{16}$ e$^-$/m^2).

To map the VTEC to the STEC, different mapping functions can be used. The empirical mapping function introduced by Lear[13] is the adopted to VTEC to STEC mapping function in this paper, however, with a minor modification. The original mapping function introduced by Lear is expressed as,

$$m(\varepsilon) = \frac{2.037}{\sqrt{\sin^2(\varepsilon) + 0.076} + \sin(\varepsilon)}, \quad [27]$$

where ε is the elevation angle of the GNSS satellite with respect to the receiver. While the original formulation of the Lear mapping function works fine for most of the cases, it only considers positive elevation angles, where in action, negative elevations are possible for spaceborne receivers. Figure 1 illustrates that while less probable than positive elevations, negative elevation angles remain a possibility.

To account for negative elevation angles, the following modified Lear mapping function is adopted.

$$m(\varepsilon) = \frac{2.037}{\sqrt{\sin^2(\varepsilon) + 0.076} + \sin(|\varepsilon|)}, \quad [28]$$

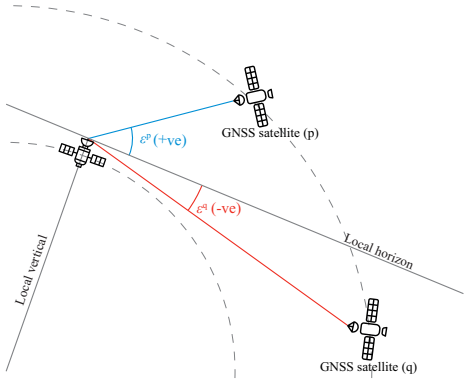

Fig. 1: Illustration of negative elevations for spaceborne receivers

5. Filter operation

In order for the EKF to operate properly, it needs an initial guess for the state vector as well as the estimated states variance-covariance matrix. The state variables where initiated with randomly selected values within the true range of each variable, and the estimation covariance matrix was inaugurated as a diagonal matrix with large variances to reflect the uncertainties of the initial guess of the state vector. It is of a huge importance to re-initiate the values of $\boldsymbol{V}_c$, $\boldsymbol{V}_t$, and $\Delta \boldsymbol{N}$ to account for newly tracked satellites. Once a value is initialized, the corresponding process noise variance needs to be set to a large value in the process noise variance-covariance matrix $\mathbb{Q}$. Moreover, a proper rearrangement of the estimated state variance-covariance matrix needs to be carried out in order to account for the satellites that went out of sight.
Besides the initialization of the state vector and the estimated states variance-covariance matrix, two other variance-covariance matrices need to be defined for the EKF to operate efficiently, the process noise variance-covariance matrix $\mathbb{Q}$ and the observation variance-covariance matrix $\mathbb{R}$.

The process noise variance covariance matrix $\mathbb{Q}$ is set to the following semi-definite time-varying matrix,

$$\mathbb{Q} = \begin{bmatrix} \mathbb{0} & \mathbb{0} & \mathbf{0} & \mathbf{0} & \mathbb{0} & \mathbb{0} & \mathbb{0} \\ \mathbb{0} & \mathbb{Q}_{\Delta \boldsymbol{v}} & \mathbf{0} & \mathbf{0} & \mathbb{0} & \mathbb{0} & \mathbb{0} \\ \mathbf{0} & \mathbf{0} & 0 & 0 & \mathbf{0} & \mathbf{0} & \mathbf{0} \\ \mathbf{0} & \mathbf{0} & 0 & \sigma^2_{c\Delta\dot{\delta}t} & \mathbf{0} & \mathbf{0} & \mathbf{0} \\ \mathbb{0} & \mathbb{0} & \mathbf{0} & \mathbf{0} & \mathbb{Q}_{\boldsymbol{V}} & \mathbb{0} & \mathbb{0} \\ \mathbb{0} & \mathbb{0} & \mathbf{0} & \mathbf{0} & \mathbb{0} & \mathbb{Q}_{\boldsymbol{V}} & \mathbb{0} \\ \mathbb{0} & \mathbb{0} & \mathbf{0} & \mathbf{0} & \mathbb{0} & \mathbb{0} & \mathbb{Q}_{\Delta \boldsymbol{N}} \end{bmatrix}, \quad [29]$$

where $\mathbb{Q}_{\Delta \boldsymbol{N}}$ is generally a matrix of zeros, except when a newly tracked satellite is introduced, then

the corresponding diagonal entry is set to a large value to reflect the unreliability of the corresponding initiated ΔN value. The state variables' noises are assumed uncorrelated, thus all the covariance elements of the $\mathbb{Q}$ matrix are zero. Furthermore, the process noise variance-covariance matrix is in general a time-varying matrix, as the entries $\mathbb{Q}_{\boldsymbol{V}}$ and $\mathbb{Q}_{\Delta \boldsymbol{N}}$ need constant rearrangement as new satellites are being tracked. The diagonal entries for $\mathbb{Q}_{\Delta \boldsymbol{v}}$, $\mathbb{Q}_{\boldsymbol{V}}$, and $\mathbb{Q}_{\Delta \boldsymbol{N}}$ are defined as,

$$
\begin{aligned}
Q_{\Delta \boldsymbol{v}}|_{i,i} &\coloneqq \sigma^2_{\Delta \boldsymbol{v}} \\
Q_{\boldsymbol{V}}|_{i,i} &\coloneqq \begin{cases} \sigma^2_{\boldsymbol{V}} & C_i \text{ tracks existing sat.} \\ 100\sigma^2_{\boldsymbol{V}} & C_i \text{ tracks new sat.} \\ 0 & \text{Otherwise} \end{cases} \\
Q_{\Delta \boldsymbol{N}}|_{i,i} &\coloneqq \begin{cases} 100 & C_i \text{ tracks new sat.} \\ 0 & \text{Otherwise} \end{cases},
\end{aligned}
\qquad [30]
$$

where C_i is the i^{th} independent channel of the GNSS receiver

Assuming uncorrelated measurement noises, the observation noise variance-covariance matrix is set to the following time-varying matrix,

$$
\mathbb{R} = \begin{bmatrix} \mathbb{R}_{SDGR} & \mathbb{0} & \mathbb{0} \\ \mathbb{0} & \mathbb{R}_{SDCP} & \mathbb{0} \\ \mathbb{0} & \mathbb{0} & \mathbb{R}_{SDGF} \end{bmatrix}, \qquad [31]
$$

where $\mathbb{R}_{SDGR}$, $\mathbb{R}_{SDCP}$, and $\mathbb{R}_{SDGF}$ are the noise variance-covariance matrices corresponding to the SDGR, SDCP, SDGF measurements respectively. Matrix $\mathbb{R}$ is time varying only as its size changes as the number of commonly tracked satellites is not constant. The off-diagonal elements of the $\mathbb{R}_{SDGR}$, $\mathbb{R}_{SDCP}$, and $\mathbb{R}_{SDGF}$ matrices are all zeros, while their diagonal elements are set to σ^2_{SDGR}, σ^2_{SDCP}, and σ^2_{SDGF} respectively.

6. Results and discussion

In order to validate the algorithm, the SWARM mission data[9] are collected to test the algorithm in a simulated real-time setting. Swarm is an Earth observation mission that consists of three identical satellites, Alpha, Bravo, and Charlie; which were launched in November 2013.

The algorithm was tested using an arbitrary 22-hours worth of GNSS data (namely on 08-Nov-2021), and the relative navigation is performed between Alpha (chaser) and Charlie (target) spacecraft which share the same orbit (170 km apart at the date of estimation).

In order for the EKF to operate efficiently, precise statistics of the process noises as well as the measurement noises need to be provided. A particular issue that needs to be addressed here is that, although the SDCP is considered a smooth signal with a noise level of order of millimeters, it cannot be considered very smooth in this context as the ionospheric model is not accurate to the millimeters order due to the varying solar activity over the years and the atmospheric variations over the alternating day and night. The statistics that were adopted are presented in the Table 2.

Qty	Value	Qty	Value
$\sigma_{\Delta \boldsymbol{v}}$	0.01 m/s^2	σ_{SDGR}	$3/\sqrt{2}$ m
$\sigma_{c\Delta\dot{\delta}t}$	1 m/s	σ_{SDCP}	0.4 m
$\sigma_{\boldsymbol{V}}$	10^{-16} TECU/s	σ_{SDGF}	$3\sqrt{2}$ m

Table 2: Statistics used in the simulation

The simulation results are illustrated in Figures 2 and 3.
Figure 2 depicts the relative position error, while Figure 3 shows the relative velocity error between the two spacecraft. It is important to note that the relative position vector $\Delta \boldsymbol{r} = \begin{bmatrix} \Delta x & \Delta y & \Delta z \end{bmatrix}^\intercal$ as well as the relative velocity vector $\Delta \boldsymbol{v} = \begin{bmatrix} \Delta v_x & \Delta v_y & \Delta v_z \end{bmatrix}^\intercal$ are both estimated in the ECEF frame, and not in the Local Vertical Local Horizontal (LVLH) frame of the target. Nonetheless, a transformation between the two frames is simple given the absolute position of the target at each time step.

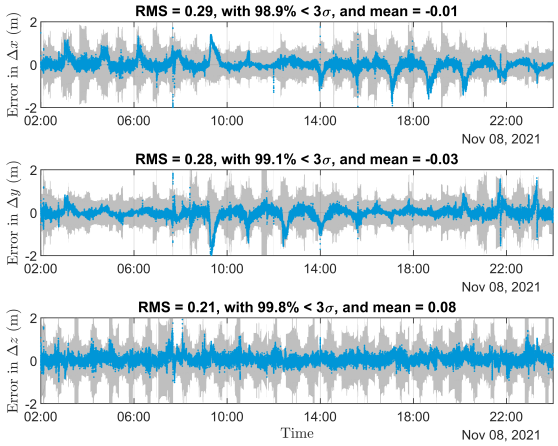

Fig. 2: Relative position error in the ECEF frame

In order to generate the error signals in Figures 2 and 3, a ground truth of the estimated states must

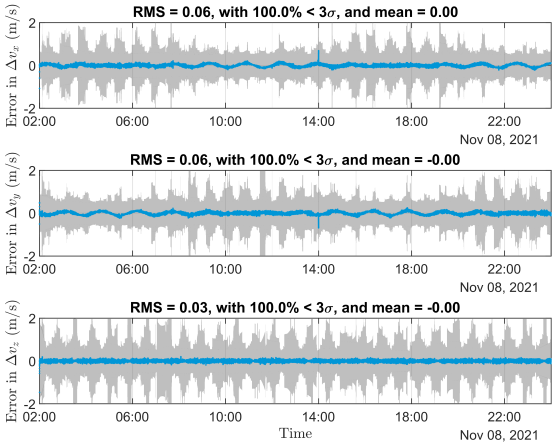

Fig. 3: Relative velocity error in the ECEF frame

be present. The output of the post-processing Precise Orbit Determination (POD) algorithms is used as the ground truth. The POD output is accurate to the level of 1-cm and is provided as part of the swarm mission data.

It is important to mention that Root Mean Square (RMS) errors of 46 cm and 9 cm/s could be obtained for relative distance and relative speed respectively, while the filter converged after 9 iterations. The convergence point in this setting is defined as the first filter iteration at which the signal is less than or equal to the RMS.
Results with such convergence rate and accuracy, especially without implementing any integer ambiguity resolution technique, could only be obtained thanks to the incorporation of the presented measurement setting and ionospheric model.

Although the obtained results are adequate for an algorithm that does not resolve ambiguities, one cannot ignore that less than 99.7% of the estimates' errors are lying within the $\pm 3\sigma$ bounds, as seen by Fig. 2. This can be justified by the inaccurate model and observation variance-covariance matrices, $\mathbb{Q}$ and $\mathbb{R}$. It is hypothesised that if the matrix $\mathbb{R}$ is formed in such a way that leverages its dependence on the elevation angles of the tracked satellites, better estimates will be obtained for both the state variables as well as the estimations variance-covariance matrix. It is also hypothesised that better estimates can be obtained if an efficient outlier detector is adopted. Our future work shall not only include a different setting for the variance-covariance matrices and outliers detection, but also include an ambiguity resolution technique on top of the EKF.

7. Conclusion

In this paper, the problem of GNSS-based relative navigation between two spacecraft with large inter-satellite distance is addressed. A measurement setting comprising the Single Difference GRAPHIC (SDGR), the Single Difference Carrier Phase (SDCP), and the Single Difference Geometric Free (SDGF) combinations is proposed. Although the classical Extended Kalman Filter (EKF) was used, augmenting the measurement vector with the SDGF combination proved to provide better estimates than that of using the classical observables such as the SDGR and the SDCP.
In order to obtain acceptable convergence rates, an ionospheric model had to be adopted instead of performing model-less estimations of the ionospheric delays. The Lear mapping function, which maps from the Vertical Total Electron Content (VTEC) to the Slant Total Electron Content (STEC), was modified in order to account for negative elevation angles of satellites with respect to receivers.
The implemented EKF could achieve 46 and 9 cm/s RMS errors in the estimated relative distance and relative speed respectively for the two SWARM mission satellites, Alpha and Charlie, which were 170 km apart at the time of estimation, which is much better than the best -to the authors' knowledge- space-borne single-frequency standalone positioning results of 1 m 3D RMS error for absolute positioning for TerraSAR-X mission.[16] It is important to emphasise that the obtained results could be achieved without implementing integer ambiguity resolution. An interesting future research path is to implement integer ambiguity resolution in conjunction with the proposed filter settings.

Acknowledgment

This work is supported by the Luxembourg National Research Fund (FNR) – AuFoSat project, BRIDGES/19/MS/14302465.

References

[1] G. S. Bhushana Rao. Ionospheric delay estimation for improving the global positioning system position accuracy. *IETE Journal of Research*, 54(1):23–29, 2008.

[2] F. D. Busse, J. P. How, and J. Simpson. Demonstration of adaptive extended kalman filter for low-earth-orbit formation estimation using CDGPS. *Journal of the Institute of Navigation*, 50(2):79–94, 2003.

[3] T. E. Carter. State transition matrices for terminal rendezvous studies: brief survey and new example. *Journal of Guidance, Control, and Dynamics*, 21(1):148–155, 1998.

[4] X.-W. Chang, X. Yang, and T. Zhou. MLAMBDA: A modified LAMBDA method for integer least-squares estimation. *Journal of Geodesy*, 79(9):552–565, 2005.

[5] W. Clohessy and R. Wiltshire. Terminal guidance system for satellite rendezvous. *Journal of the Aerospace Sciences*, 27(9):653–658, 1960.

[6] N. A. Correa-Muños and L. A. Cerón-Calderón. Precision and accuracy of the static gnss method for surveying networks used in civil engineering. *Ingeniería e Investigación*, 38(1):52–59, 2018.

[7] S. D'Amico, J.-S. Ardaens, and O. Montenbruck. Navigation of formation flying spacecraft using gps: the prisma technology demonstration. In *Proceedings of the 22nd International Technical Meeting of the Satellite Division of The Institute of Navigation (ION GNSS 2009)*, pages 1427–1441, 2009.

[8] T. Ebinuma, O. Montenbruck, and E. Lightsey. Precise spacecraft relative navigation using kinematic inter-spacecraft state estimates. In *Proceedings of the 15th International Technical Meeting of the Satellite Division of The Institute of Navigation (ION GPS 2002)*, pages 2038–2046, 2002.

[9] European Space Agency. SWARM mission data. `https://earth.esa.int/eogateway/missions/swarm/data`, 2022.

[10] V. Giralo and S. D'Amico. Precise real-time relative orbit determination for large-baseline formations using gnss. In *Proceedings of the 2021 International Technical Meeting of The Institute of Navigation*, pages 366–384, 2021.

[11] R. Kroes, O. Montenbruck, W. Bertiger, and P. Visser. Precise grace baseline determination using gps. *Gps Solutions*, 9(1):21–31, 2005.

[12] A. Le and C. Tiberius. Gps standard positioning service: how good is it? *European Journal of Navigation*, 1(2):21–27, 2003.

[13] W. Lear. Gps navigation for low-earth orbiting vehicles. *1st rev., NASA Rept*, 1987.

[14] A. Leick, L. Rapoport, and D. Tatarnikov. *GPS satellite surveying*. John Wiley & Sons, 2015.

[15] S. Leung and O. Montenbruck. Real-time navigation of formation-flying spacecraft using global-positioning-system measurements. *Journal of Guidance, Control, and Dynamics*, 28(2):226–235, 2005.

[16] O. Montenbruck, Y. Yoon, E. Gill, and M. Garcia-Fernandez. Precise orbit determination for the terrasar-x mission. In *Proceedings of the 19th International Symposium on Space Flight Dynamics*, 01 2006.

[17] T. Takasu and A. Yasuda. Kalman-filter-based integer ambiguity resolution strategy for long-baseline rtk with ionosphere and troposphere estimation. In *Proceedings of the 23rd international technical meeting of the satellite division of the institute of navigation (ION GNSS 2010)*, pages 161–171, 2010.

[18] P. Teunissen. The least-squares ambiguity decorrelation adjustment: A method for fast gps ambiguity estimation. *Journal of Geodesy*, 73:587–593, 1999.

[19] T. P. Yunck. Coping with the atmosphere and ionosphere in precise satellite and ground positioning. *Washington DC American Geophysical Union Geophysical Monograph Series*, 73:1–16, 1993.